CHAPTER II
LITERATURE REVIEW

2.1 Lithium-ion Batteries (LIBs)

Lithium-ion batteries (LIBs) are widely well-known as rechargeable batteries or secondary batteries because of their electrically reversible electrochemical reactions. There are several different combinations of chemicals are generally used, including: lead acid, nickel cadmium (NiCd), nickel metal hydride (NiMH), lithium ion (Li-ion) (Broussely and Archdale, 2004). They are acceptable market leaders in clean energy storage technologies with a number of efforts consisting of their relatively high energy-to-weight ratios, lack of memory effect, low self-discharge rate and long life. Due to theirs high energy density and high discharge voltage (Dong *et al.*, 2011; Lee *et al.*, 2012; Wang *et al.*, 2012), they are widely used in electric vehicles (EVs), hybrid-electric vehicles (HEVs) and portable applications such as digital cameras, laptops, mobile phones etc (Yuan *et al.*, 2011).

Lithium-ion batteries generally comprise of three primary functional components: a cathode, an anode, and an electrolyte. The chemical reaction takes place inside a lithium-ion battery during charge and discharge operation. Lithium ions are extracted from the anode during discharging, moved through the electrolyte and inserted into the cathode. Meanwhile electrons flow through an external circuit from the same direction, generating electrical power. On the other side, both lithium ions and electrons are transported back in the opposite direction by an applied external voltage, storing electrical energy as chemical energy in the battery for next usability (Mukherjee *et al.*, 2011; Song *et al.*, 2011).

Performance of the anode and cathode are generally quantified in terms of capacity per unit mass or per unit area of the electrode material, where capacity is the total number of ampere-hours that can be withdrawn from a fully charged cell under specified conditions of discharge. In general, the different types of cathode materials, anode materials, electrolytes and the rate of charge/discharge (C-rate)

exhibit considerably influence on the nature of insertion and extraction of Li^+ ion, the operating voltage, capacity and also cycle life.

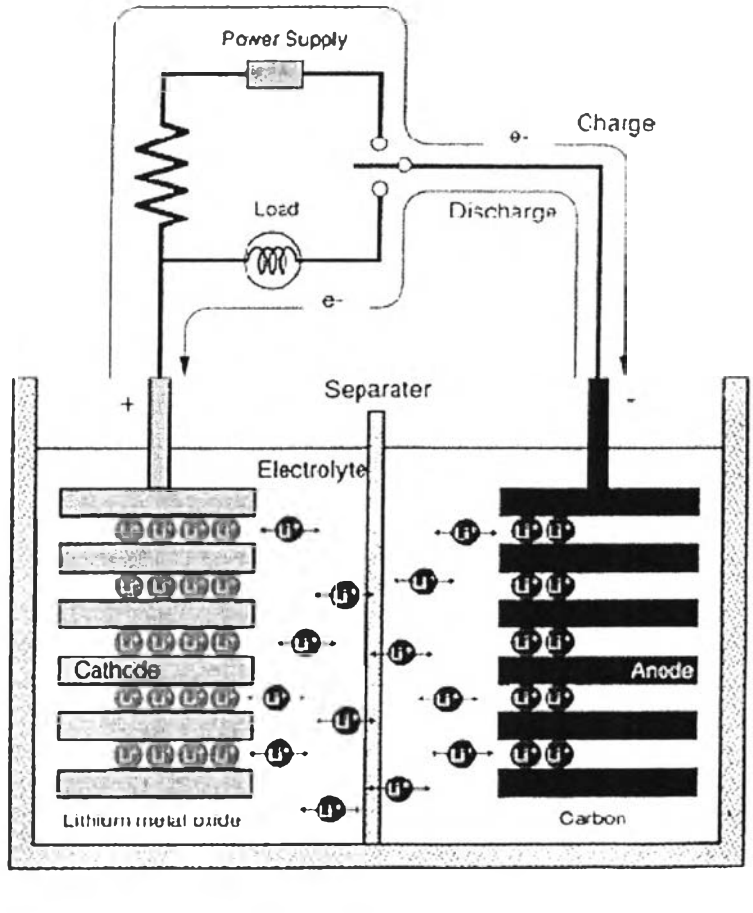

Figure 2.1 Lithium-ion cell operation, during charging lithium ions intercalate into the anode, the reverse occurs during discharge (Wakihara, 2001).

2.2 Materials for Lithium-ion Batteries

2.2.1 Cathode Materials

The performance of cathode materials is largely dominated by the structural stability and conductivity of cathodes (Mukherjee *et al.*, 2011). Thus, the principle characteristics required for efficient cathode materials are as follow: (Wakihara, 2011).

a) Gibbs free energy of the discharge reaction ought to have large negative (high discharge voltage).

b) The host structure must have low molecular weight and the capability to accommodate large amount of reversible intercalation and deintercaltion of lithium and lithium ion diffusivity (high energy capacity).

c) The host structure must have high lithium chemical diffusion coefficient (high power density).

d) The structural modifications should be as small as possible during lithium intercalation and deintercalation (long cycle life).

e) Chemical stable, non-toxic and inexpensive needed for cathode materials.

f) Materials should have the ease of handling.

Cathode materials are primarily categorized into three different types; lithium metal oxides, spinels, and lithiummetal phosphates.

2.2.1.1 Lithium Metal Oxides

Among the cathode materials for lithium-ion batteries, $LiCoO_2$ is the most widely used and dominated the lithium battery market, with a theoretical capacity of 273 $mAhg^{-1}$. $LiCoO_2$ offers significant advantages regarding the ease of synthesis, high working potential, excellent cycle ability at room temperature, and low self-discharge. Nevertheless, limitations of $LiCoO_2$ cathodes still exist. First, cycling of $LiCoO_2$ cathodes is limited to a cut-off voltage of about 4.2 V, corresponding to a reversible delithiation of 0.5 Li. In addition, this limitation causes the attained practical capacity from the cathode to only about half of its theoretical capacity. Moreover, cycling at voltages above 4.2 V has lead to the structural degradation and dissolution of cobalt into the electrolyte that finally restricts cycle ability. Second, $LiCoO_2$ is limited due to a relatively low diffusion coefficient with respect to the slow solid state diffusion of Li^+ cations within them and lastly $LiCoO_2$ is highly toxic and also expensive (Dong *et al.*, 2011; Mukherjee *et al.*, 2011).

2.2.1.2 Spinels

For the purpose of discounting cost and improving the safety characteristics, $LiMn_2O_4$ spinel has been investigated as an appealing alternative material for cathodes because of its abundance, less expensive, excellent thermal stability, and environmental friendly. However, capacity fading associated with other

factors such as structural changes, slow manganese dissolution in the electrolyte during the cycling, lattice distortions, and microstrain force spinel cathodes confronted considerable limitations.

2.2.1.3 Lithium Metal Phosphates

On account of their low cost, low toxicity, and long cycle life, $LiFePO_4$ cathodes, with a theoretical capacity of 170 $mAhg^{-1}$, provide numerous benefits over cobalt oxide or even spinel based materials. Charging and discharging mechanisms of $LiFePO_4$ are shown in eq. 1 and 2, respectively.

$$LiFePO_4 + xLi^+ + xe^- \rightarrow xFePO_4 + (1-x)LiFePO_4 \quad (1)$$

$$FePO_4 + xLi^+ + xe^- \rightarrow xLiFePO_4 + (1-x)FePO_4 \quad (2)$$

The excellent reversibility during extended cycling has been attributed to similarities in the structures of $LiFePO_4$ and $FePO_4$. The major drawback of $LiFePO_4$, however, is poor lithium ion conductivity and poor electronic conductivity. When the particle size is reduced, the lithium ion diffusion length in the structure inclines to be effectively reduced leading to obstruct its application in high power batteries (Mukherjee *et al.*, 2011; Song *et al.*, 2011).

2.2.2 Electrolyte Materials

The cell voltages given in the electrochemistry section are larger than the potential at which aqueous solutions can electrolyze, in addition lithium is highly reactive to water; therefore, aqueous electrolytes cannot be used due to their possible decomposition. Consequently, non-aqueous or aprotic solutions are used as possible electrolytes. To be a good electrolyte, such a non-protonic electrolyte must have a good ionic conductivity, high chemical stability, safety, and low cost.

2.2.2.1 Liquid Electrolytes

Liquid electrolytes in lithium-ion batteries consist of lithium salts, such as $LiPF_6$, $LiBF_4$ or $LiClO_4$ in an organic solvent, such as ethylene carbonate (EC), dimethyl carbonate (DMC), and diethyl carbonate (DEC). A liquid electrolyte conducts lithium ions, acting as a carrier between the cathode and

the anode when a battery passes an electric current through an external circuit. The operation temperature of lithium-ion batteries is usually between -20 °C and +60 °C; therefore, solvents with low melting point, high boiling point, and low vapor pressure are extremely desirable. In addition to these requirements, the ionic conductivity of Li^+ ion is also concerned which is proportional to its mobility, the number of mobile ions, and viscosity resulting in the ease of ion movement (Wakihara, 2011). Unfortunately, organic solvents easily decompose on anodes during charging. However, when inappropriate organic solvents are used as the electrolyte, the solvent decomposes on the graphite surface during the first cycle and forms a solid layer called the solid electrolyte interphase (SEI), which is electrically insulating yet, affects the irreversible capacity, sufficient ionic conductivity, the self-discharge, the cycle life, and the safety (Tasaki *et al.*, 2009; Verma *et al.*, 2011). SEI is a very complicated layer consisting of inorganic components which are normally salt degradation products and organic components which are partial or complete reduction products of the solvent of the electrolyte.

SEI components are highly temperature sensitive. Thus, performance of the batteries even at high/low temperature relies on the SEI. However the most vital outcome of SEI is on the safety of the batteries. Besides, there is the study of factors which contribute to properties of the SEI comprising of type of carbon, pretreatment of carbon, electrolyte composition, and the electrochemical conditions (Verma *et al.*, 2011).

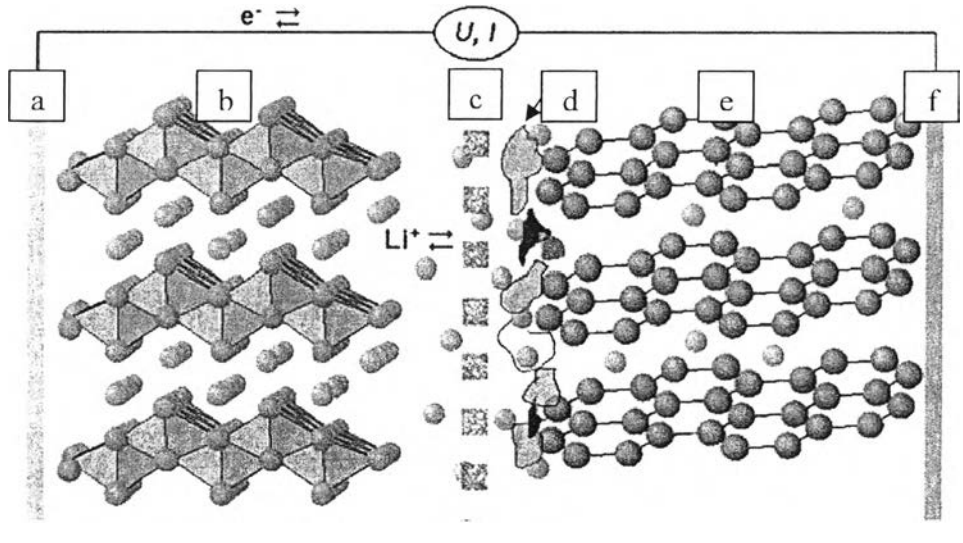

Figure 2.2 Schematic illustration of a typical Li-ion battery: (a) Aluminum current collector; (b) Oxide active material; (c) Porous separator soaked with liquid electrolyte; (d) Inhomogeneous SEI layer; (e) Graphite active material and (f) Copper current collector (Verma *et al.*, 2011).

2.2.2.2 Polymer Electrolytes

As the result that related to the safety of the batteries, there are many attempts to revise the weaknesses of liquid electrolytes. Thus, polymer electrolytes, or solid electrolytes, have been widely developed thanks to their advantages over liquid electrolytes such as, good chemical and mechanical stability. A new class of solid polymer electrolytes developed which mixed lithium salts in poly(ethylene oxide) (PEO) which called intrinsic (dry) solid polymer electrolytes (SPEs). Local relaxation and segmental motion of the host polymer chains (SPE) (see in Figure 4.) allows the movement of a dissolved lithium salts and ionic conduction between the electrodes while at same time provides and insulating barrier to electronic conduction and physical separation of the positive and negative electrodes resulting in high conductivity of electrolytes. There also are other examples of intrinsic (dry) solid polymer electrolytes such as, polyether, polyester, polyamind, polysulfide, etc.

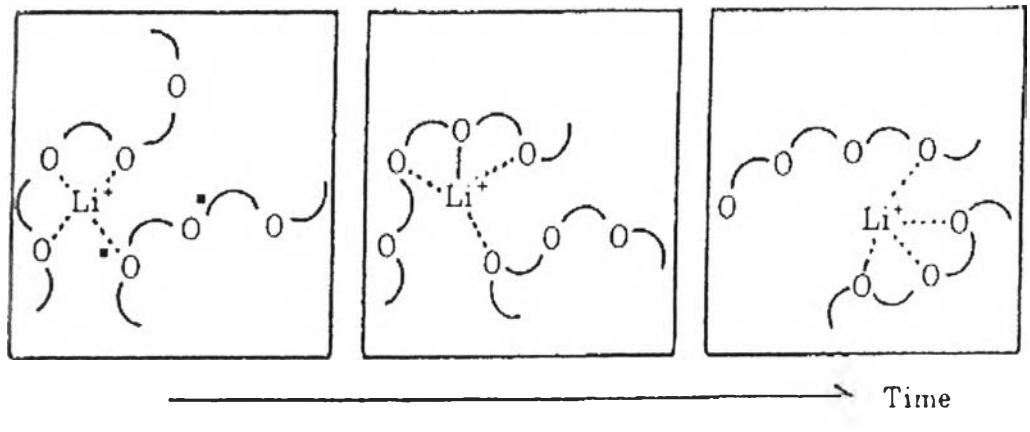

Figure 2.3 Mechanism of Li^+ ion conduction in intrinsic (dry) SPE (Wakihara, 2001).

2.2.2.3 Gel-type Solid Polymer Electrolytes

Gel-type SPE contains a small amount of appropriate organic solvent known as a plasticizer which creates two effects to polymer. First, it makes segmental motion easier and another is liquid-like character can be offered. These effects provide enhancement of ionic conductivity of gel-type SPE. Some host polymers used for gel-type SPE are polyacrylonitrile, polyvinylidene fluoride, poly(ethylene oxide), poly(propylene oxide), and so on.

Normally, polymer electrolytes have some imperfections of the conductivity which is lower than liquid electrolytes and limitation of invalid convey high power at room temperature and especially, low temperature batteries. Nonetheless, they also have various strong points composed of more safety and ease of battery fabrication in different shapes (Dong *et al.*, 2011; Wakihara 2011).

2.2.3 Anode Materials

Anode materials are primarily classified into three different types; lithium metal and carbonaceous materials, lithium alloying compounds and intermetallic alloys, and transition metal compounds.

2.2.3.1 Lithium Metal and Carbonaceous Materials

Although, metallic lithium has very high energy density (3860 $mAhg^{-1}$), the operational safety problem is going to be concerned related to its low melting point (approximately 180 °C), dendrite growth during charge/discharge cycling, and high reactivity toward electrolytes. The required properties of anode materials continue to have attention with the goal of developing materials capable of absorbing lithium reversibly. Thus, the usage of lithium insertion compounds like carbonaceous materials are gained more favor to use instead of metallic lithium (Song *et al.*, 2011). Carbonaceous materials can be commonly classified into (1) graphite, (2) non-graphitized glass-like carbon (hard carbon) which is directly pyrolyzed from solid phase, and (3) soft carbon, obtained from liquid or gas phase, easily changeable with heat treatment (Liu *et al.*, 2011; Wakihara, 2011).

Figure 2.4 Three types of carbon (Wakihara, 2001).

In general, hard carbon and graphite are employed to use as anodes to ensure stable capacity during cycling. Due to the natural structure of graphite that consists of ABAB layers, which are held together by van der Waals forces; lead it deserving a significant role for lithium intercalation to allow ease of insertion and deinsertion of Li^+ ions [13]. Graphite compounds exhibit a theoretical capacity of 372 $mAhg^{-1}$ of carbon corresponding to the formation of LiC_6 which on delithiation as shown in eq. 3: (Mukherjee *et al.*, 2011).

$$Li^+ + 6C + e^- \leftrightarrow LiC_6 \quad (3)$$

Since then, the performances of lithium storage compounds have been necessarily improved, including energy density, rate capability, cycle stability cost, and environmental benign (Ji *et al.*, 2010) to replace graphite-based anodes which have limited available of a theoretical capacity of 372 $mAhg^{-1}$ and low Li^+ ion diffusion between carbon layers (Wakihara, 2011).

2.2.3.2 Lithium Alloying Compounds and Intermetallic Alloys

The alternative anode materials capable of inserting lithium ions have been explored in order to achieve higher performance that lead to the development and utilization of a wide variety of lithium alloying systems. Examples include metals that can store a large amount of lithium through the formation of

alloys like $Li_{4.4}Si$, $Li_{4.4}Ge$, $Li_{4.4}Al$, $Li_{4.4}Sn$, and Li_3Sb. Though, lithium alloys show a high capacity of about 900-4,000 $mAhg^{-1}$ (Mukherjee *et al.*, 2011), they still have the major problem which related to their tremendous volume expansion and contraction from lithium insertion/deinsertion, which takes place during the charging and discharging process. This may cause the pulverization of the electrode materials and poor cycling performance.

2.2.3.3 Transition Metal Compounds

The conversion reactions have been used to produce nanocomposite electrode capable of storing lithium. In this process, a compound MX (where M represents a 3D transition metal and X represents O, F, N or S) is reduced by Li to the metal M and a corresponding lithium compound as follows in eq. 4:

$$M_mX_n + 2nLi^+ + 2ne^- \leftrightarrow nLi_2X + mM \quad (4)$$

This conversion reaction provides the merit of allowing the storage of more than two lithium ions per molecule, potentially offering high capacity and good reversibility (Song *et al.*, 2011). Among transition metal compounds, metal oxides can significantly prolong cycle life because of the formation of a Li_2O buffering matrix upon electrochemical reaction or favorable crystal structure for lithium insertion (Wang *et al.*, 2012).

The enhanced electrochemical reactivity of Li_2O is attributed to the unique nanostructure, consisting of uniformly dispersed nano-sized (around 5 nm) transition metal phase and lithium oxides, which has large contact areas and very short diffusion paths for both Li^+ ions and electrons diffusion.

At present, the usage of nano-sized transition metal oxides show excellent electrochemical performance, however, their application in practical lithium-ion batteries is strongly hampered with respect to their high synthesis cost, relatively poor rate capability (or power density), low volumetric density, poor long-term cycling stability (Song *et al.*, 2011). Thus, for the next generation lithium-ion batteries, much effort is loaded to conquer the drawbacks of anode materials.

2.3 Electrospinning Process

Electrospinning technique is a simple and versatile method for a fiber-formation process capable of producing continuous nanoscale-diameter fibers using electrostatic forces. In the electrospinning process, electric field is subjected to the end of a capillary tube that contains the polymer fluid held by its surface tension and finally induces a charge onto liquid polymer solution surface. The droplet will experience two types of electrostatic forces: electrostatic repulsion between the charges on the surface and Coulombic forces in the external field. Under the influence of these two forces, the droplet will be elongated and finally deformed into conical shape, typically referred to as Taylor cone (see Figure 2.5). When the applied voltage reaches a critical value, the electric field strength overcomes the surface tension, and a charged jet of fluid will be ejected. On the contrary, if the applied voltage is not high enough, the jet will break up into droplets, a phenomenon called Rayleigh instability (Chronakis, 2010). Thus, the polymer solution must have a concentration high enough to cause polymer entanglements yet not so high that the viscosity prevents polymer motion induced by the electric field. The solution must also have a surface tension low enough, a charge density high enough, and a viscosity high enough to prevent the jet from collapsing into droplets before the solvent has evaporated (Frenot and Chronakis, 2003).

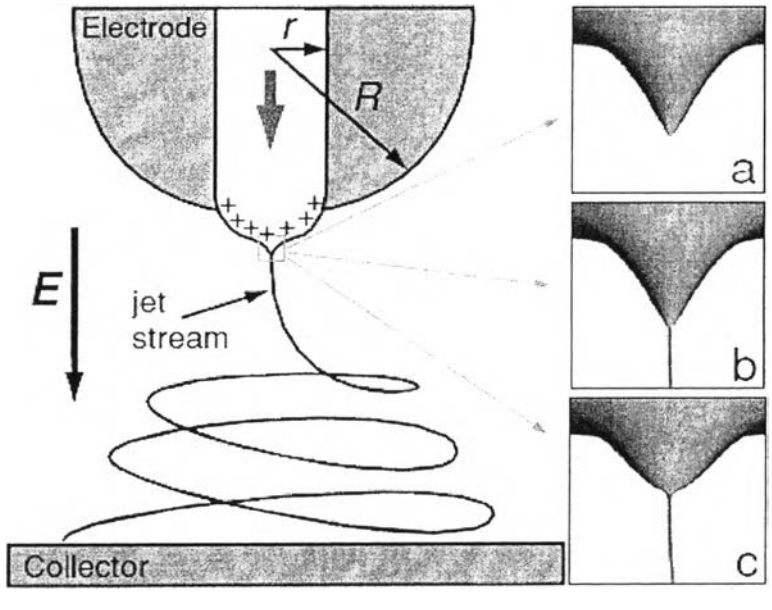

Figure 2.5 Schematic representation of an electrospinning apparatus (r, radius of the capillary; R, curvature radius of the electrode used) and Taylor cones. (a) Formation of Taylor cone in an applied electric field. (b) Taylor cone ejects fluid jet. (c) Surface tension causes cone shape to relax. Jet stream starts out in stable straight region, then becomes unstable, partly owing to charge repulsion, typically showing a whipping or spiraling motion (Burger *et al.*, 2006).

The electrically charged jet undergoes a series of electrically induced deviations from a linear to a curvilinear configuration, known as bending instabilities, during its passage to the collection screen, which results in the polymer being deposited on the grounded collector via a whipping motion (see figure 2.6). Since the charged jet accelerates towards regions of lower potential, the solvent evaporates rapidly, and the resulting increase in the electrostatic repulsion of the charged polymer causes the fibers to elongate and lay themselves randomly on a grounded collecting metal screen. The rapidly whipping jet, the fluid instability, is a crucial constituent of the process that causes bending and stretching of the jet.

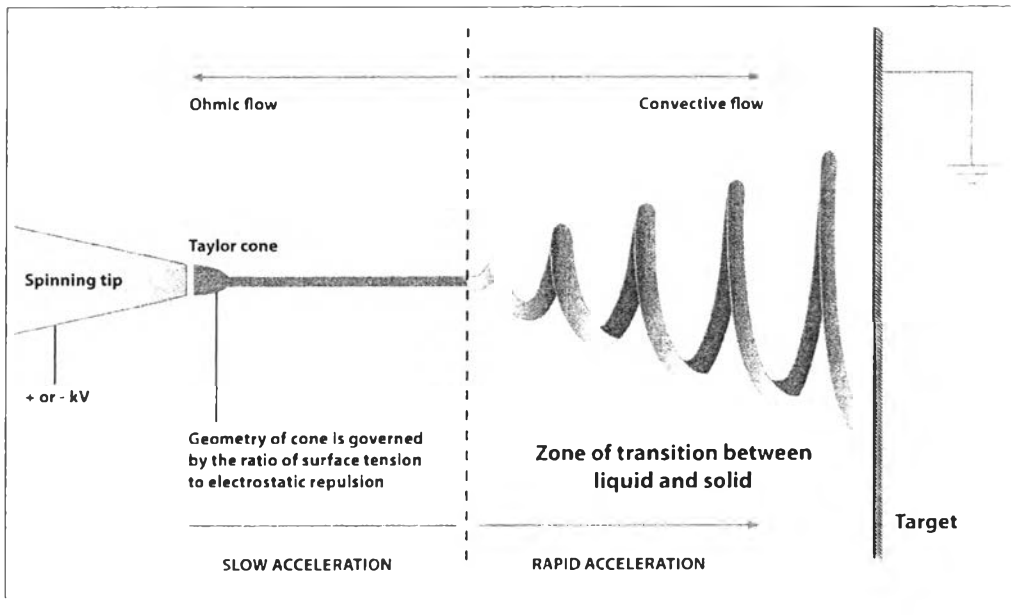

Figure 2.6 Whipping motion occurred in rapid acceleration zone. (http://en.wikipedia.org/wiki/Electrospinning, 8 September 2008)

2.3.1 Electrospinning Apparatus

The typical laboratory setup for electrospinning apparatus consists of a spinneret (typically a hypodermic syringe needle) connected to a high-voltage direct current power supply, a syringe pump, and a grounded collector.

The polymer solution or melt is loaded into the syringe which is a glass tube. A metering pump attached to the plunger of the syringe generates a constant pressure and flow of the fluid through the syringe. But a metering pump is essential for low viscosity feedstocks. The driving force is provided by a high voltage source which is applied between the syringe nozzle and a collector. Electrospinning is fundamentally different from air or other mechanically driven spinning techniques in that the extrusion force is generated by the interaction between the charged polymer fluid and an external applied electric field (Dong *et al.*, 2011).

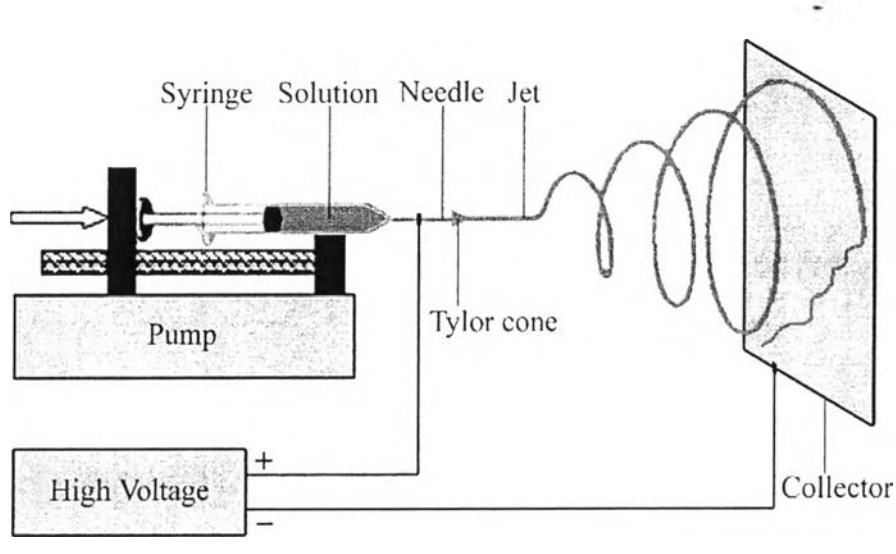

Figure 2.7 A schematic of an electrospinning setup (Ziabari *et al.*, 2009).

2.3.2 Modeling of Electrospinning Process

The process of electrospinning consists of three stages: (1) jet initiation and jet thinning, so-called jet diameter; (2) jet elongation; (3) solidification of jet into nanofibers.

2.3.2.1 Jet Initiation

Generally, a pendent droplet of polymer solution is carried by surface tension at the tip of spinneret. When the droplet is subjected to an external electric field, a charge is induced on the surface of the droplet. This charge offsets the forces of surface tension and the droplet changes shape from spherical to conical shape, referred to as the Taylor cone. When the intensity of the applied electric field reaches a certain critical value, the electrostatic forces at the surface overcome the force associated with surface tension of the polymer solution and force the ejection of the liquid jet from the tip of the Taylor cone. The highest charge density is present at the tip of the cone from where the jet is initiated. The more potential goes up, the more charge density and the flow rate of the jet increase.

There are parameters that impact the electrospinning process, such as solution concentration, field strength, flow rate, specific surface area, jet velocity and so on. In the case of low molecular weight fluids, the radius decay of an electrostatically driven jet depends on the flow rate of the polymer solution. The radius of the jet decreases slowly with the fast flow rate fast. The ratio of surface area to volume (specific surface area) is inversely proportional to the jet radius as shown in eq. 5. Therefore, an increase in the jet radius results in a corresponding decrease in the specific surface area associated with that specific volume element.

$$\frac{A}{V} = \frac{2}{R} \tag{5}$$

Where A is the surface area of the cylindrical volume element, V is the volume, and R is the radius of the jet.

If consider about the effect of the acceleration of the fluid, it has been found that a decrease in the acceleration of the fluid results in an increase in jet radius. Because the density of the polymer solution and the surface charge density are assumed to be constant, then it follows that the charge to mass ratio will decrease with increasing jet radius. The acceleration is directly proportional to the ratio of charge to mass as seen from eq. 6.

$$a = E\left(\frac{q}{m}\right) \quad (6)$$

Where *a is* acceleration, E is the electric field strength, q is the available charge for the given volume element, and m is the mass of a given volume element (Garg and Bowlin, 2011).

Solution concentration has also been found to most strongly affect fiber size, with jet diameter increasing with increasing solution concentration according to a power law relationship (Frenot and Chronakis, 2003). Moreover, the jet diameter decreases with the distance from the orifice, lower electric field and a higher surface tension coefficient. Both higher and lower viscosity can cause a thinner jet (Chronakis, 2010).

2.3.2.2 Jet Elongation

After jet initiation, the traveling liquid jet is subjected to a variety of forces with different effects as a result of various fluid instabilities which occur in this stage. Three different instabilities were identified: the classical (axisymmetric) Rayleigh instability, electric field induced axisymmetric instability and whipping instabilities (Frenot and Chronakis, 2003). Rayleigh instability occurs due to opposing forces acting on the surface area of the jet resulting in the jet to break up into droplets and if chain molecules are not present or are not long enough to prevent droplet break up, discrete spherical droplets are also formed.

Nevertheless, the key element in reducing the jet diameter from micrometer to nanometer is considered by a nonaxisymmetric or whipping instability, which causes bending or stretching of the jet. The bending allows large elongation and thinning of the fiber to occur. So, the time is necessary for the rearrangement of the excess charge along the length of the jet to get longer. The location of the excess charge then inclines to change with the elongation. The jet will be elongated in the direction of its axis by the repulsive Coulomb forces between the charges carried with the jet as far as the jet solidifies.

2.3.2.3 Jet Solidification

The solidification of the jet results in the deposition of dry nanofibers on the collector. The variations that influence on the solidification rate of

the jet are the polymer concentration, electrostatic field, and gap distance. Solidified jets can form fibers that are attached at points of contact partially by the conglutination process. Strong attachments at crossing points are an important factor in determining the mechanical properties of the nonwoven structure due to their ability to stiffen the materials up. After the initial bending instability, the jet path may follow a very complicated path and successive loops of coil may touch in flight and form permanent connections to be network form is called a garland (Garg and Bowlin, 2011).

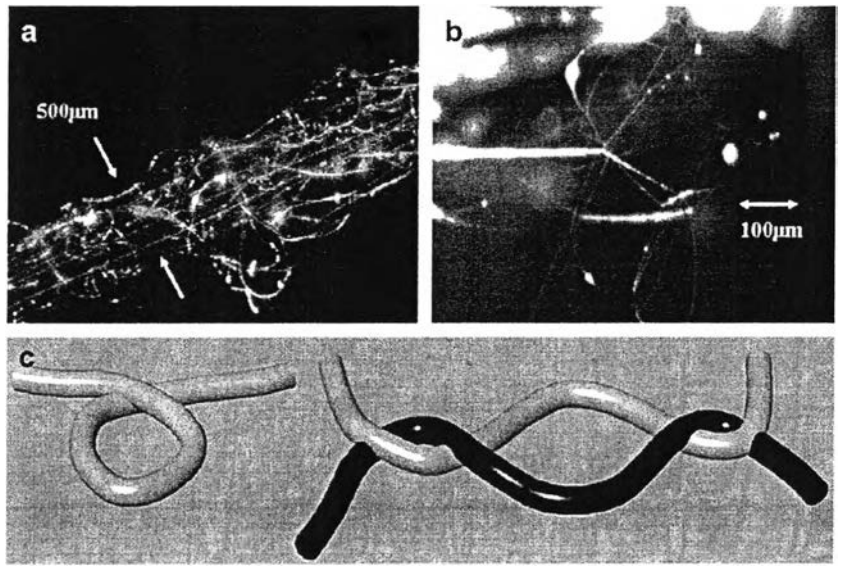

Figure 2.8 Illustrations of (a) A short segment of a garland yarn, (b) Details of the conglutinated solid fibers, and (c) A diagram of a loop in a segment of one fiber and another loop (Garg and Bowlin, 2011).

2.3.3 Parameters of Electrospinning Process

The transformation of polymer solutions into nanofibers in the electrospinning process is governed by many parameters. These parameters include:

a) System parameter such as properties of polymer solution (viscosity, polymer concentration, conductivity, surface tension, and dielectric

constant), polymer rheology, molecular weight, molecular weight distribution, and volatility of solvents.

b) Process parameter such as field strength applied voltage, flow rate, distance between the tip and collector, needle tip design and placement, collector composition and geometry and take up velocity of the collector.

c) Ambient parameters such as temperature, humidity and at mospheric pressure.

For instance, overabundant flow rates results in generating fibers with beads, since they do not have sufficient time to dry before drifting toward the collector. Temperature can cause the decrease in the viscosity of polymer solutions which leads to the reduction of fiber diameter. With respect to distance between the tip and the collector, morphological changes can occur. Consequently, an optimum distance is required between the tip and the collector to allow adequate time for fibers to dry before stretching onto the collector. At distances that are either too close or too far, bead formation has been observed. Applied fields can, moreover, influence the morphology, creating a variety of new shapes on the surface (Kulkarni *et al.*, 2011).

2.3.4 Coaxial Electrospinning

Recently, there are several innovative electrospinning processing techniques to enhance the function and properties of electrospun fibers such as, forced air assisted electrospinning, air-gap electrospinning, mixed electrospinning, etc. Coaxial electrospinning is one of innovative electrospinning processing techniques which allow two polymer solutions can be coelectrospun without direct mixing, using two concentrically aligned nozzles. The principle of this fiber formation technique is similar to normal electrospinning process as aforementioned. But coaxial nanofibers contained cylindrical core-shell morphology can be created. Removal, e.g. by dissolution with a selective solvent, of the core from such a coaxial nanofiber leads to ultimately acquire hollow nanofibers.

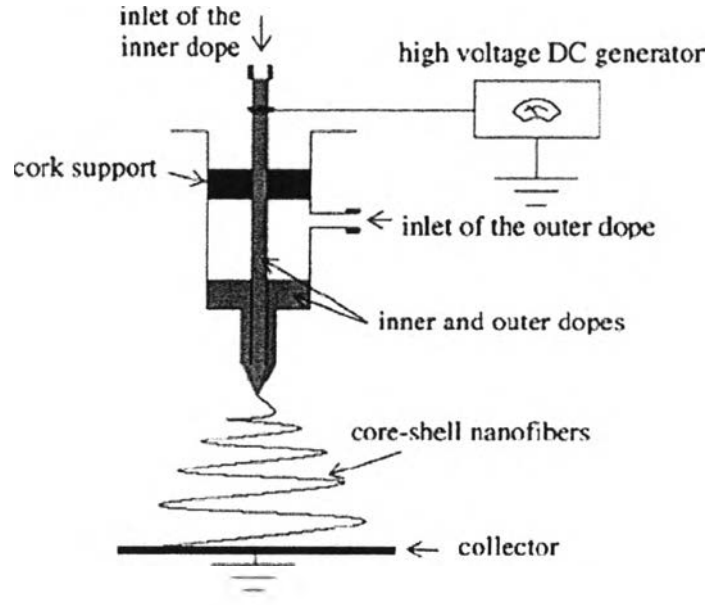

Figure 2.9 The experimental setup of coaxial electrospinning (Garg and Bowlin, 2011).

Overall, this technique can be useful in producing different types of dual composition nanofibers, functional graded nanocomposites, surface-modified nanofibers, and continuous hollow nanofibers. These resulting core-shell structures can also be used for bioactive tissue scaffolds, highly sensitive biochemical sensors, and drug controlled-released (Garg and Bowlin, 2011).

In 2010, Liu et al. fabricated a novel core-shell coaxial carbon nanofibers web (C-CNFW) from the mineral oil (core)/PAN (sheath) nanofibers through a coaxial electrospinning method and subsequently thermal treatments.

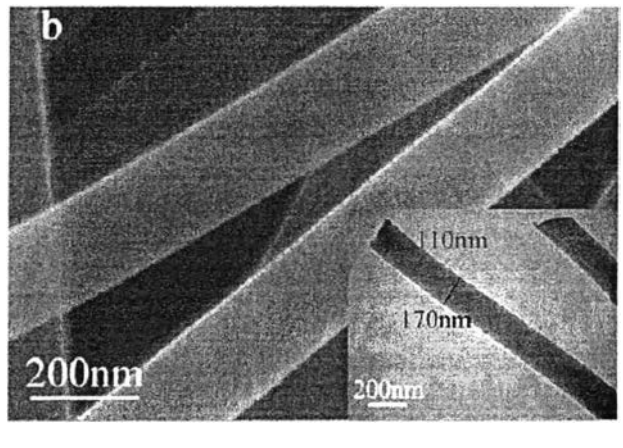

Figure 2.10 High-magnification SEM micrographs and TEM images inserts of C-CNFW carbonized at 850 °C.

in 2012, Lee *et al.* studied the influence of the carbonization temperature on turbostratic carbon structures and electrochemical properties of hollow carbon nanofibers (HCNFs) used as anode materials in LIBs. Various HCNFs are successfully synthesized using co-axial electrospinning of styrene-co-acrylonitrile (core) and PAN (shell) solutions and subsequent thermal treatments.

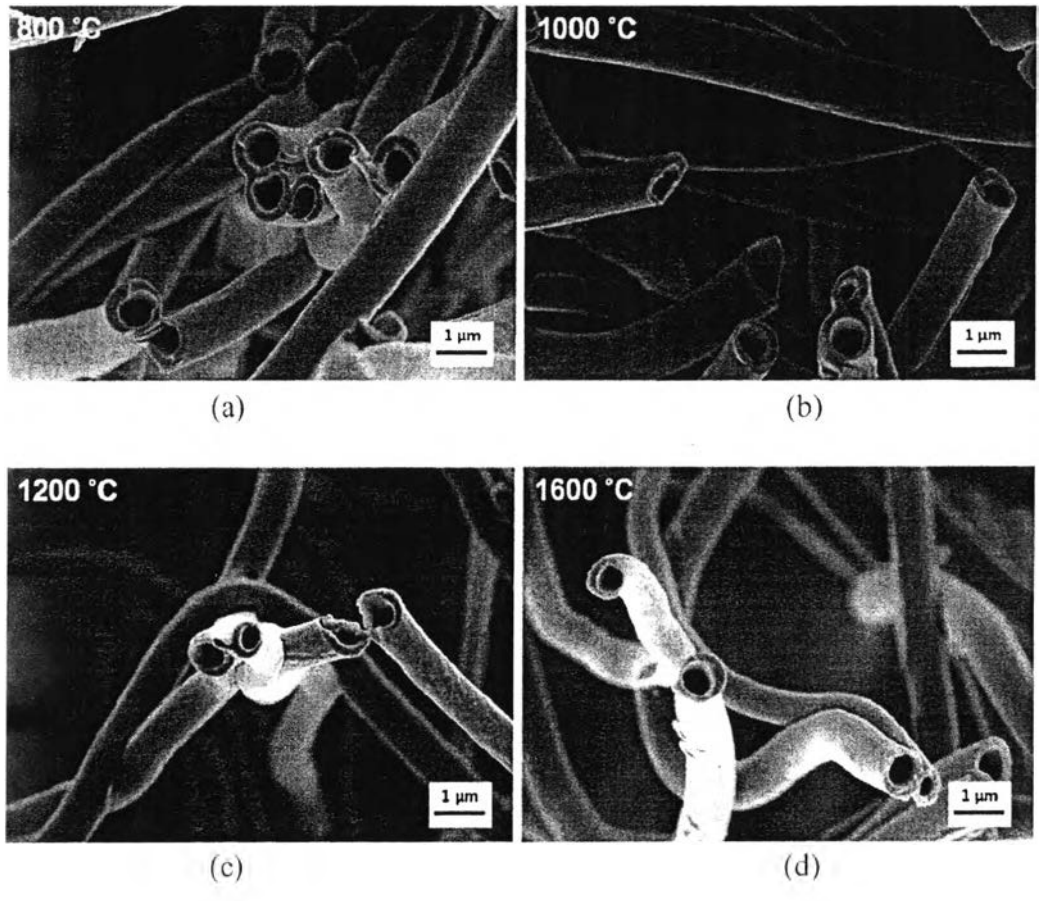

Figure 2.11 FE-SEM images of HCNFs carbonized at various carbonization temperatures: (a) 800, (b) 1000, (c) 1200, and (d) 1600 ˚C.

2.4 Hydrothermal Synthesis

Hydrothermal synthesis is a process that utilizes single or heterogeneous phase reactions in aqueous media at elevated temperature (T>25°C) and pressure (P>100 kPa) to crystallize ceramic materials directly from solution. The process is usually conducted in steel pressure vessels called autoclaves with or without teflon liners under controlled temperature and/or pressure with the reaction in aqueous solutions. The temperature can be elevated above the boiling point of water, reaching the pressure of vapor saturation. The temperature and the amount of solution added to the autoclave largely determine the internal pressure produced. Although upper limits of hydrothermal synthesis extend to over 1000°C and 500 MPa pressure, practically, temperature and pressure restrictions fall around 350°C and 100 MPa. However, mild conditions are preferred for commercial processes which below reaction conditions and severe conditions are preferred for processes which above that ones. The transition from mild to severe conditions is determined mostly by corrosion and strength limits of the materials of construction that comprise the hydrothermal reaction vessels. In the process, some factors need to be considered in different materials. In the case of hydrothermal growth of single crystals, additional pressure adjustment is done to control solubility and growth rate. Reactants used in hydrothermal synthesis are generally called precursors, prepared in the form of solutions, gels, and suspensions. Mineralizers are either inorganic or organic additives that are often used to control pH but are used at excessively high concentrations (e.g., 10 M) to also promote solubility. Other additives, also organic or inorganic, are used to serve other functions such as promote particle dispersion or control crystal morphology (Riman *et al.*, 2002).

2.5 Crystal Growth and Nucleation

Basically, crystal is a solid material composed of atoms, molecules, or ions arranging in order and repeating in pattern. The process of crystal formation is called crystallization or solidification. In general, there are two main stages to grow; nuclation and growth stages. Nucleation and growth continue to occur

simultaneously while the supersaturation appears. Supersaturation is the driving force of the crystallization; therefore, the rate of nucleation and growth is driven by the existing supersaturation in the solution.

2.5.1 Nucleation

The formation of a new crystalline from a solution begins via the nucleation process. Nucleation is the process whereby a small nucleus, such as a dust particles, a tiny sedd crystal, called cluster containing the newly forming crystal is created. The newly produced crystal comes from atoms or molecules of a reactant phase rearrange into a cluster of the product phase large enough to grow irreversibly toward a macroscopically larger size. Nucleation occurs relatively slowly as the initial crystal components. Nucleation can be either homogeneous, in the absence of foreign particles or crystals in the solution, or heterogeneous, in the presence of foreign particles in the solution. Typically, heterogeneous nucleation takes place more quickly than homogeneous one due to the influence of foreign particles which act as a starter for the crystal to grow on. Both types of nucleation are well known as primary nucleation which is the initial formation of a crystal where there are no other crystals present or where, if there are crystals present in the system, they do not have any influence on the process. In case of secondary nucleation, it is defined as the formation of nuclei attributable to the influence of the existing of crystals in the substance.

2.5.2 Crystal Growth

After crystal nucleation stage, the second stage of growth rapidly occurs. Crystal growth is the processes by which an atom or a molecule is incorporated into the surface of a crystal and extended outwards from the nucleating site, where the few crystal molecules that have bonded together begin the growth phase. During the growth phase, the prearranged pattern of atom repetitions, begins to become evident and ultimately result in a rise in size. These different processes can be briefly summarized into four steps illustrated in Figure 2.12:

1) transport of atoms through solution;

2) attachment of atoms to the surface;

3) movement of atoms on the surface;

4) attachment of atoms to edges and kinks.

The first process is the so-called transport process, while 2–4 are related to surface processes and may involve several substeps (Cubillas and Anderson, 2010).

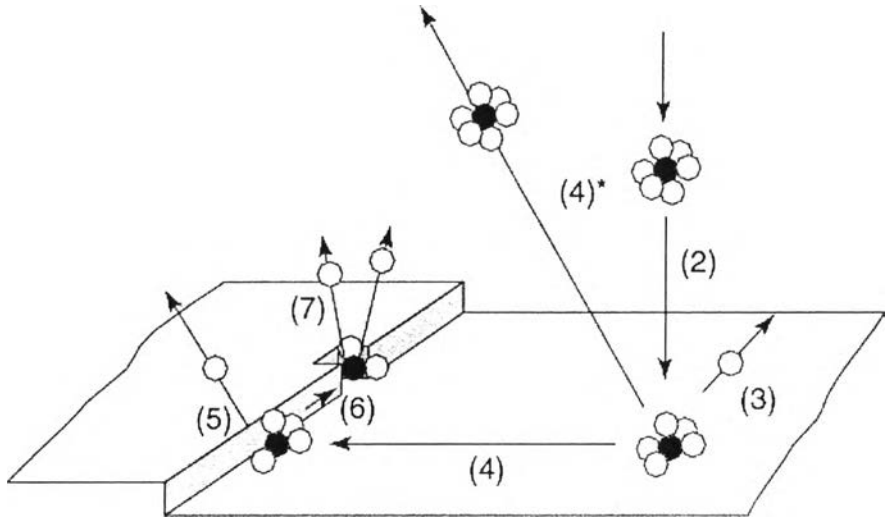

Figure 2.12 Schematic representation of processes involved in the crystal growth: (1) Transport of solute to a position near the crystal surface; (2) diffusion through boundary layer; (3) adsorption onto crystal surface; (4) diffusion over the surface; (4*) desorption from the surface; (5) attachment to a step or edge; (6) diffusion along the step or edge; (7) Incorporation into kink site or step vacancy.

2.6 Nanofibrous Materials

Nanostructured fibrous materials have drawn a lot of attention owing to their outstanding characteristics to be optimal candidates for various value added applications such as medical, filtration, energy storage, nanosensors, cosmetic, tissue engineering scaffolds, and also military protection clothing. The nonwoven structure has unique features, including flexibility in surface functionalities, interconnected pores, a very large surface-to-volume ratio (this ratio for a nanofiber can be as large as 10^3 times of that of a microfiber) and superior mechanical performance (e.g. stiffness and tensile strength) compared with any other known form of the materials.

Highly porous fabrics obtained from depositing as nonwoven fabrics, i.e., they have a large interconnected void volume in the range of 50% to even greater than 90% and also have the outstanding feature of the highest surface-to-volume ratios among all cohesive porous materials. Their structures bonded together by entangling fibre or filaments referred to the entangled fibrous geometry which has a pseudo-bicontinuous structure. The pore volume is essentially continuous and interconnected, meanwhile woven fabrics compartmentalize the pore volume more regularly. The mechanical stability of nonwoven structures, which depends on the chemical composition and processing procedure, can be improved further. For example, the crossing points of those fibers can be annealed and attached together (Burger *et al.*, 2006).

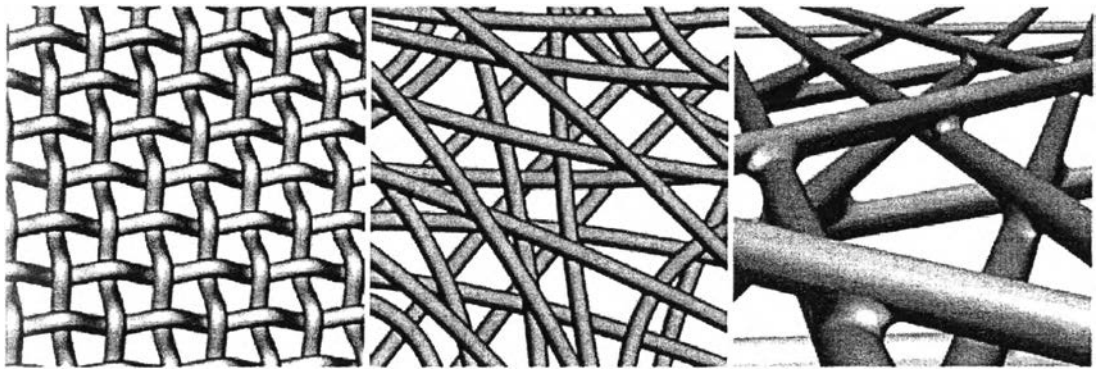

(a) Woven fabrics (b) Nonwoven fabrics (c) "Soldered" junctions

Figure 2.13 Artistic representations of (a) Woven fabrics, (b) Nonwoven fabrics (c) nonwoven electrospun mat detail visualizing a soldering-like attachment (Burger *et al.*, 2006).

In recent years, nanofibrous materials can be created in a wide variety of ways such as drawing, template synthesis, self-assembly, phase separation, electrospinning, lithography etc. There are several different in strong and weak points of each process as shown in Table 2.1 (Huang *et al.*, 2003).

Table 2.1 Advantages and disadvantages of each process for fiber-formation

process	advantages	disadvantages
drawing	-Ability to make one-by-one very long single nanofibers	-Undergoing of strong deformations only in a viscoelastic material
template synthesis	-Ability to make nanometer tubules and fibrils of raw materials	-Inability to make one-by-one very long single nanofibers
self-assembly	-Ability to organize themselves into desired patterns and functions in suitable condition	-Taking long period of time in processing continuous polymer nanofibers
phase separation	-Ability to form a nano-porous foam	-Taking long period of time to transfer the solid polymer into the nano-porous foam
Electrospinning	-Ability to one-by-one continuous nanofibers from various polymers - Ability to control fiber diameter and morphology -Ease of processing -Low cost	- Having a lot of parameters concerned in the process

2.7 The Development of Electrospun Fibrous Anode Materials in Lithium-ion Batteries.

Some of the major challenges facing the advancement of the current lithium-ion battery technology can be briefly described as follows (Song *et al.*, 2011):

(1) The obtainable capacity is insufficient (and lower than the theoretical ones) and declines with the rate of cycling.

(2) Inadequacy of the power density (or rate capability).

(3) The energy efficiency is too low due to large polarization losses for charge and discharge, more so at higher cycling rates.

(4) The cycling life is limited owing to capacity fading with cycling.

Therefore, several anode materials have been developed with desirable electrochemical properties in order to overcome some critical problems and satisfy many requirements in LIBs. Nonetheless, plentiful of challenges still remain in the development of anode materials for a new generation of lithium-ion batteries. They are explained below.

2.7.1 Lithium Metals

Even if lithium metals have very high theoretical energy density, they have been dominated by the formation of lithium during charge/discharge process. Partial shorting of the two electrodes can be occurred and may lead to eventual catastrophic failure of battery. Thus, surface modification of lithium metal electrodes represents a vast challenge to utilization of lithium metal electrodes which can minimize or exterminate dendrite formation.

Choi *et al.* (2003) produced a protection layer based on the crosslinked gel polymer electrolyte (see Figure 2.14) for the lithium electrode protection which was formed by ultraviolet (UV) radiation-curing of a mixture of crosslinking agent (1,6-hexanediol diacrylate), liquid electrolyte (ethylene carbonate (EC)/propylene carbonate (PC)/1 M $LiClO_4$), and photoinitiator (methyl benzoylformate). They proved that the introduction of a prepared protection layer contains ability for minimizing the passivation caused by the decomposition reaction of the liquid electrolyte (EC/PC/1 $LiClO_4$) on the surface of the lithium electrode and

the electrochemical performance of the lithium metal polymer battery is also enhanced The smoother surface and less porous of the solid electrolyte interphase (SEI) layer were improved by the protected layer on lithium anode during the charge–discharge runs at 1C rate resulting in minimizing of dendrite formation.

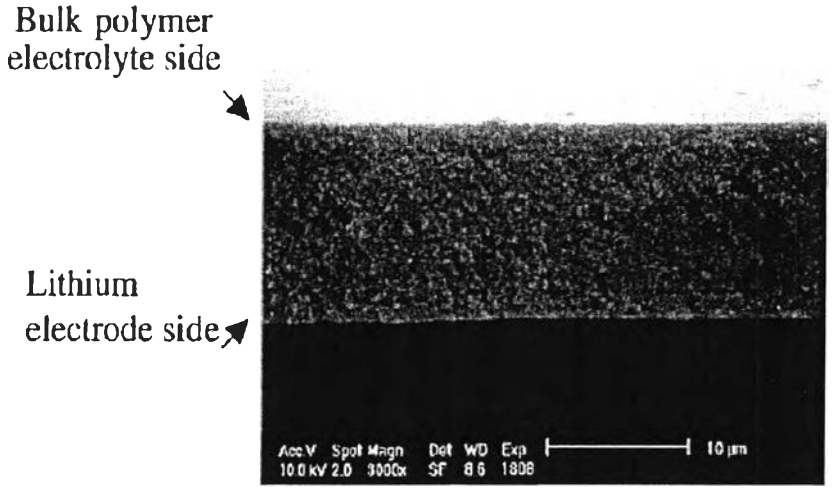

Figure 2.14 The SEM image for the cross-section of the protection layer.

2.7.2 The Low Intrinsic Electrical Conductivity of Electrode Materials

The low intrinsic electrical conductivity of active electrode materials often causes the lower practical capacities than theoretical capacities which decreases further with the rate of cycling.

In 2003, Ning *et al.* studied capacity fading of lithium-ion batteries (carbon material) cycled at high discharge rates. They have found the capacity loss of the whole battery should be directly related to the loss of lithium ions as well as individual electrode's ability to intercalate or deintercalate lithium ions. Moreover, they discovered the capacity fading increased with increasing in cycling due to the more deposition of decomposed material on the electrode surface incorporated with the formation of SEI film. Figure 2.15 and 2.16 showed SEM images of carbon materials cycled at different discharge rates and illustration of the formation of the SEI film when the battery is cycled, respectively.

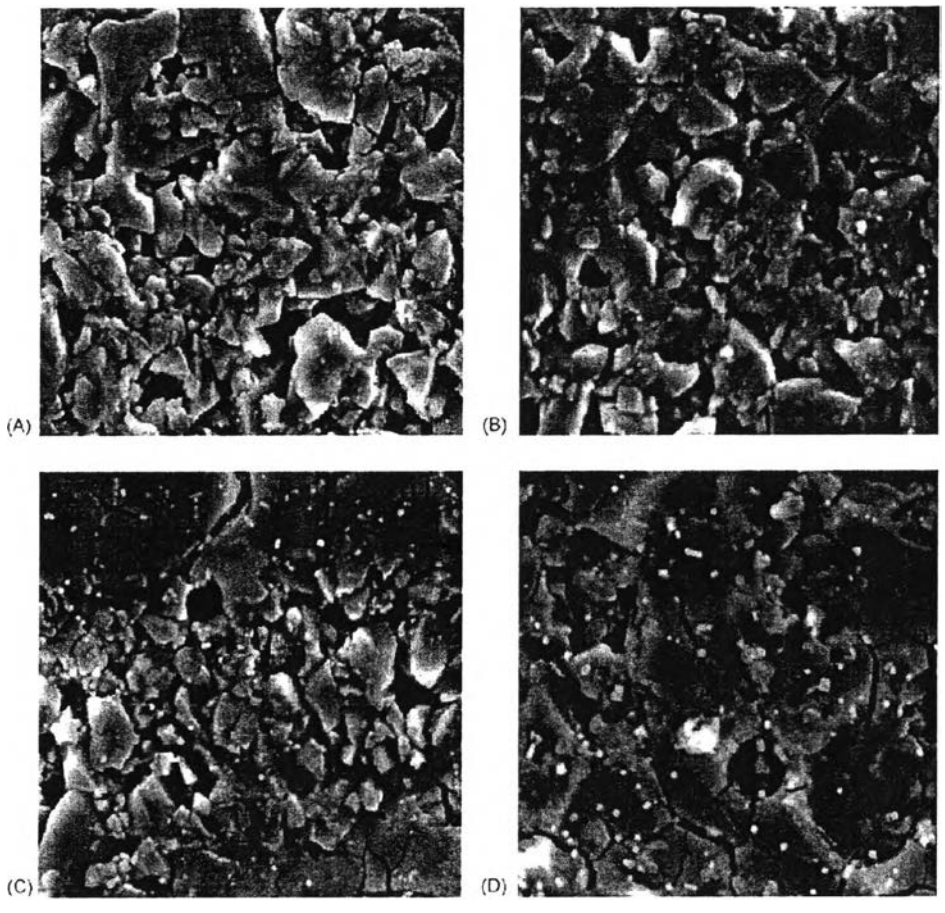

Figure 2.15 SEM (1000X) of carbon materials cycled at different discharge rates. (A) Carbon cycled at 1C; (B) carbon cycled at 2C discharge rate; (C) and (D) carbon cycled at 3C discharge rate.

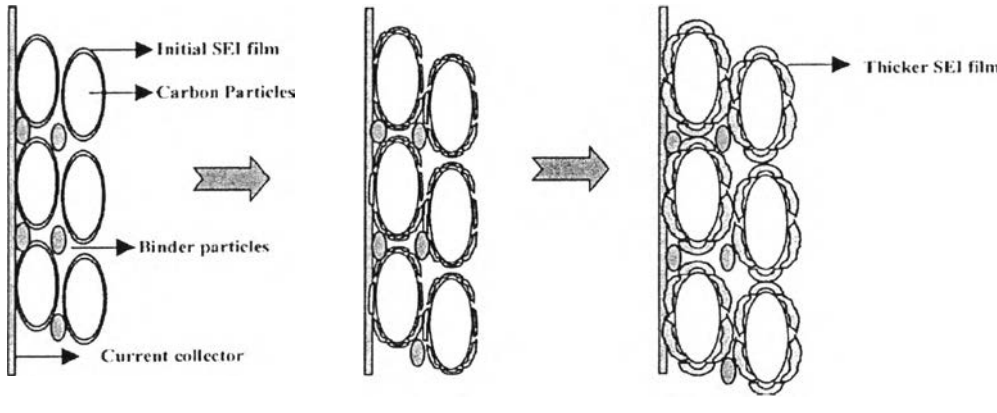

Figure 2.16 Evolution of the SEI film on the surface of carbon when the battery is continued to be cycled.

2.7.3 Transition Metal Oxides

Transition metal oxides with conversion reactions suffer from the rate capability (or power density) related to their relatively high potential (or low cell voltage) and limited lifetime due to capacity fading with cycling.

In 2010, Yang *et al.* prepared the very large area uniform SnO_2 nanofibers consisting of orderly bonded nanoparticles by thermal pyrolysis and oxidization of tin(II)2-ethylhexanoate /polyacrylonitrile (PAN) nanofibers in air via one simple electrospinning technology for the first time. These one-dimensional nanofibers are characterized by many mesoporosities in the nanofibers and nanopores between the bonded SnO_2 nanoparticles. These special structures provide a larger electrode-electrolyte contact area and enable alleviation of the mechanical strain owing to the volume changes during charge/discharge processes. They have been found that because of the enlarged surface area and pulverization during the discharge/charge process, a relatively large irreversible capacity and some extent of capacity fading will be took place.

2.7.4 Zero-strain Insertion Anode Materials

For $Li_4Ti_5O_{12}$ improved safety which is a zero-strain insertion anode due to the negligible volume change during the lithium insertion/extraction process.

In 2007, Lu *et al.* prepared 3D network architecture of anatase TiO_2 and spinel $Li_4Ti_5O_{12}$ by electrospinning process. Their results demonstrated that $Li_4Ti_5O_{12}$ exhibited a stable in 3D network architectures and good reversible in electrochemical cycles, meanwhile 3D architectures of electrospun anatase TiO_2 nanofibers were destroyed faster during Li^+ ion insertion. Thus, $Li_4Ti_5O_{12}$ can be expected to have potential application for 3D batteries as a zero-strain insertion material (structural change resistance). However, it exhibits high redox potential (about 1.5 V vs. Li/Li^+) and low capacity.

Guo *et al.* (2011), moreover, had a further improvement of the capacity of $Li_4Ti_5O_{12}$ via electrospinning process to prepare two kinds of $Li_4Ti_5O_{12}$/C composites with different morphologies ($Li_4Ti_5O_{12}$/C particles/fibers and $Li_4Ti_5O_{12}$/C fibers). They have been found that both composites provide higher reversible capacities and better rate performance than commercial $Li_4Ti_5O_{12}$ nanoparticles. In comparison to $Li_4Ti_5O_{12}$/C particles/fibers, $Li_4Ti_5O_{12}$/C fibers gave even higher

capacity, greater rate performance, smaller electrode polarization, and better kinetics which can be indicated that these improvements is attributed to the elimination of $Li_4Ti_5O_{12}$ aggregates and the fiber-formation. Some limitations still remain due to relatively large porosity which can minimize energy density for the batteries.

2.7.5 Volume Expansion and Contraction of Anode Materials

Most anode materials undergo volume expansion or contraction associated with lithium insertion/extraction leading to pulverization of active electrode materials or mechanical failure of the electrode. For instance, The Sn-based materials suffer from poor cycling performance owing to large specific volume changes and nanoparticle aggregation during repetitious insertion/de-insertion processes. Thus, many attempts have been devoted in order to accommodate the large volume changes and reduce the Sn-based particle aggregation.

In 2010, Yu *et al.* fabricated reticular tin nanoparticle-dispersed carbon (Sn/C) nanofibers via electrospinning subsequent carbonization at different temperatures. The materials carbonized at 700 and 850 °C deliver high charge (785.8 and 811 mA h g^{-1}) and discharge (1211.7 and 993 mA h g^{-1}) capacities at the first cycle. The relatively good electrochemical performance of the Sn/C nanofibers at 700 °C and 850 °C result from the combined merits of Sn (high lithium-storage capacity) and carbon matrix (stable cycling) as well as the unique feature of reticular nanofiber.

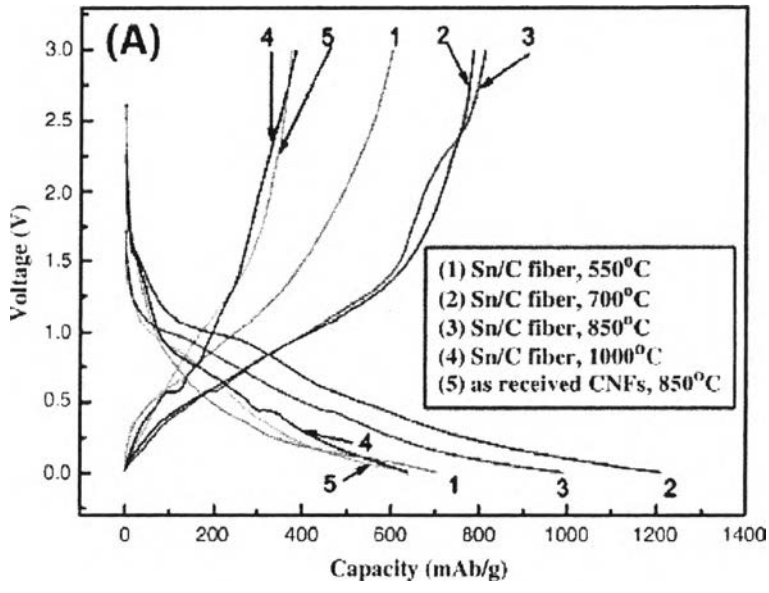

Figure 2.17 Galvanostatic discharge/charge curves for the first cycle.

2.7.6 Si-based Anodes

Si-based anodes have shown huge promising performance with the aid of various nanostructures (i.e., nanowires, 3D porous particles, and nanotubes). Nonetheless, the application to commercial batteries may obstructed by the synthesis processes usually involve low yield, complex procedures and high cost, toxic precursors. The development of large-scale, low-cost fabrication methologies for nanomaterials with satisfactory performance is one of considerable challenges in the fabrication of battery materials, such as electrospinning method.

In 2009, Ji and Zhang prepared carbon/Si composite nanofibers with porous structures by using relatively convenient and low cost electrospinning and subsequent carbonization processes (thermal treatment). They exhibit a large discharge capacity of 1100 $mAhg^{-1}$ at a high current density of 200 mAg^{-1}. As a result, it can be described that LIBs can benefit from both Si phases (large lithium storage capacity) and carbon matrix (long stable cycle life). These combined effects eventually lead to acceptable electrochemical performance at high current density.

In 2010, Wang *et al.* studied the effects of the C/Si ratio on the electrochemical performance of the obtained composite nanofibers via

electrospinning and subsequent carbonization processes. From the result, the C/Si composite nanofibers (77/23, w/w) exhibit large reversible capacity up to 1240 $mAhg^{-1}$ and stable capacity retention even in 40 cycles. The scanning electron microscopy is also used to study the morphology change during the lithium intercalation, and the result reveals that fibrous morphology can effectively protect the electrode from mechanical failure due to the huge volume expansion during lithium insertion in silicon. In contrast to their enhancement, the limitations in rate capability of the C/Si nanofibers may become an obstacle for high power lithium-ion batteries and hence they have to be further improved. The SEM image of C/Si 3.3:1 composite nanofibers cycled for 15 cycles at 0.1 C. shown in Figure 2.18.

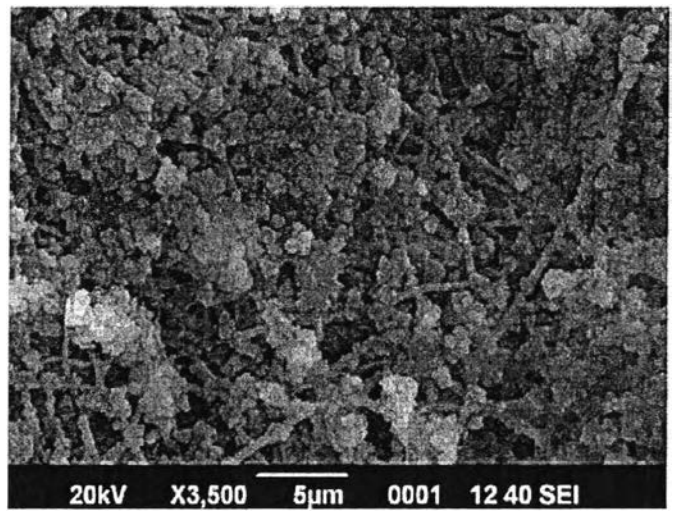

Figure 2.18 The SEM image of C/Si = 3.3:1 composite nanofibers cycled for 15 cycles at 0.1 C.

2.7.7 Other Improvements

Some recent researches are focusing on improving the battery performance by investigation and adaptation of novel structure associated with various metallic nanomaterials into either carbon nanofibers or other metal oxides nanofibers, such as TiO_2, as electrodes.

In 2008, Wang *et al.* prepared Carbon–cobalt (C/Co) composite nanofibers with diameters from 100 to 300 nm by electrospinning and subsequent

heat treatment. They discovered that Co can increase the interfacial surface area between the carbon and liquid electrolyte, and enhances the electronic conductivity. The C/Co composite nanofibers exhibit high reversible capacity (>750 $mAhg^{-1}$) and good rate capability (578 $mAhg^{-1}$ at 1 C rate) comparing to conventional graphite anodes which have a maxiumum capacity of 372 $mAhg^{-1}$.

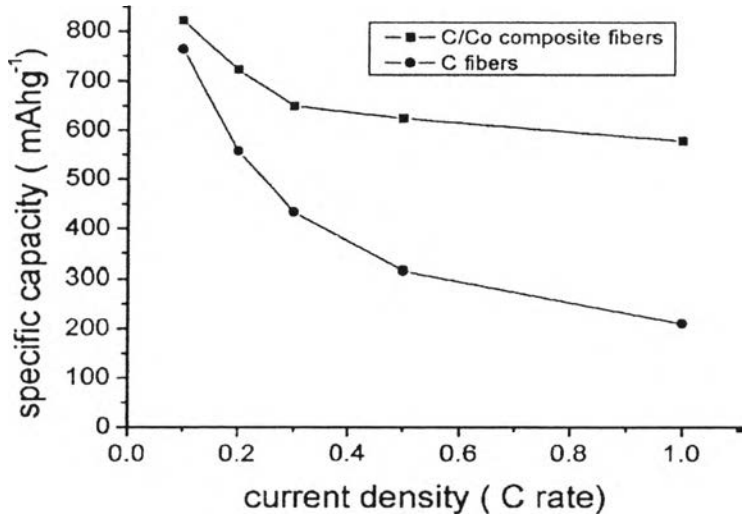

Figure 2.19 Discharge capacities of the fibers measured at different current densities from 100 to 1000 $mAhg^{-1}$.

An anode material made of Fe_3O_4/C composite nanofibers was prepared by Wang *et al.* (2008). The 600 °C-carbonized Fe_3O_4/C composite nanofiber had much better electrochemical performance with a high reversible capability of 1007 $mAhg^{-1}$ at the 80th cycle and excellent rate capability. It can be implied that the addition of Fe_3O_4 in the composite plays significant roles in increasing the effective surface area, enhancing the electronic conductivity and improving the wet ability of the electrode.

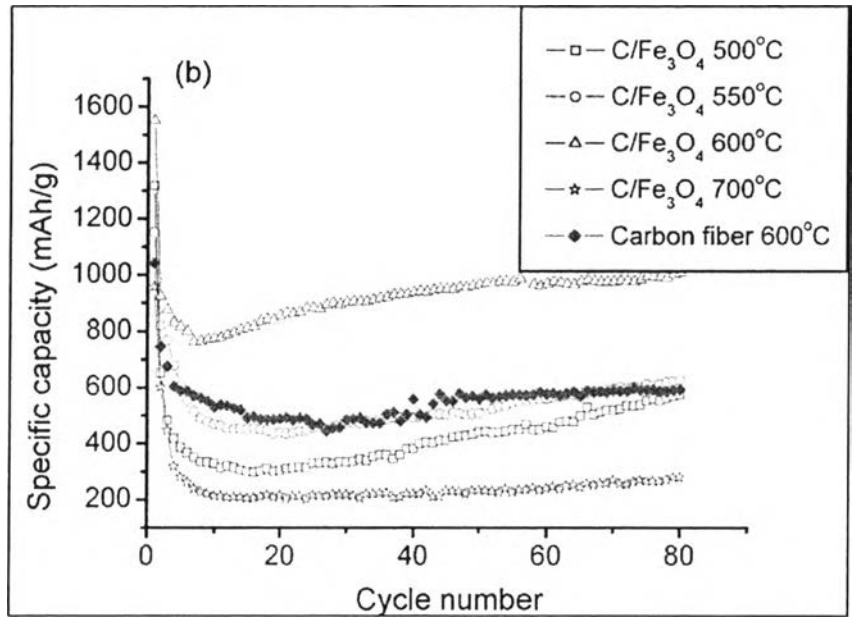

Figure 2.20 Electrochemical tests of C/Li or Fe_3O_4/C/Li half cells: discharge capacity versus cycles of the nanofibers.

In 2010, Reddy *et al.* synthesized anatase TiO_2 nanofibers by electrospinning and nanoparticles by the molten salt method. Electrochemical properties of the materials are evaluated using cyclic voltammetry, galvanostatic cycling and electrochemical impedance spectroscopy. Electrochemical characterization showed that although electrospun TiO_2 nanofibers had lower specific capacity than TiO_2 nanoparticles, their electrochemical cycling stability was higher due to the lower capacity fading of TiO_2 nanofibers (~23%) compared to that of the nanoparticles (~63%).

Nam *et al.* (2010) synthesized one-dimensional titanium dioxide (1D-TiO_2) incorporated with Au or Ag metallic nanoparticles (metallic-nanoparticle-embedded one-dimensional titanium dioxide) via electrospinning process and subsequent by calcination at high temperature of 450°C. The formation of 1D-TiO_2 nanofibers composites (Ag/1D-TiO_2 or Au/1D-TiO_2) were obtained by the thermal decomposition. The various microscopic and X-ray spectroscopic methods were employed to examine the impacts of Ag or Au incorporation. From the result, the embedded Ag or Au nanoparticles were found to affect the changes in crystallinity and size of TiO_2 after the incorporation of Ag or Au nanoparticles into

1D-TiO_2. Additionally, lithium-ion diffusion and charge transfer were promoted. In comparison to pristine 1D-TiO_2, the specific capacity of metal nanoparticle-embedded 1D-TiO_2 nanofiber composites was improved by 20% or more (see Figure 2.22), and the rate performance was improved 2-fold. Consequently, the metal nanoparticles were constructed within 1D-TiO_2 nanostructures can provide the better electrical conductivity and cycling stability of Ag/1D- TiO_2 and Au/1D- TiO_2.

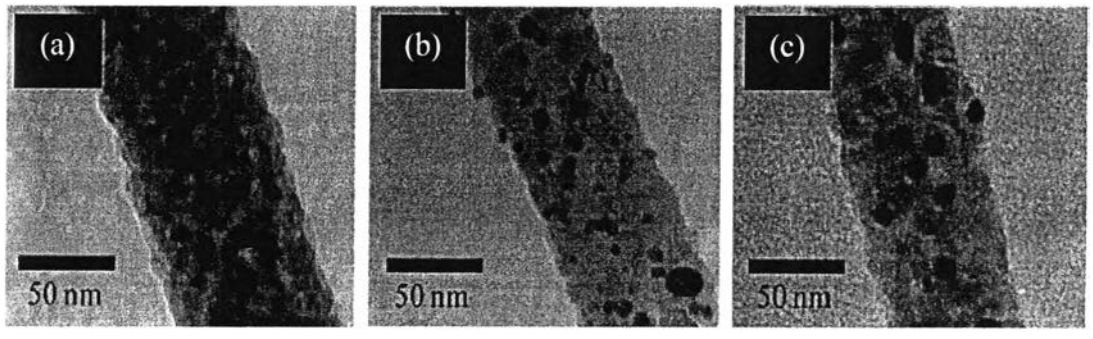

Figure 2.21 The TEM images of (a) pristine 1D-TiO_2, (b) Ag/1D-TiO_2, and (c) Au/1D-TiO_2.

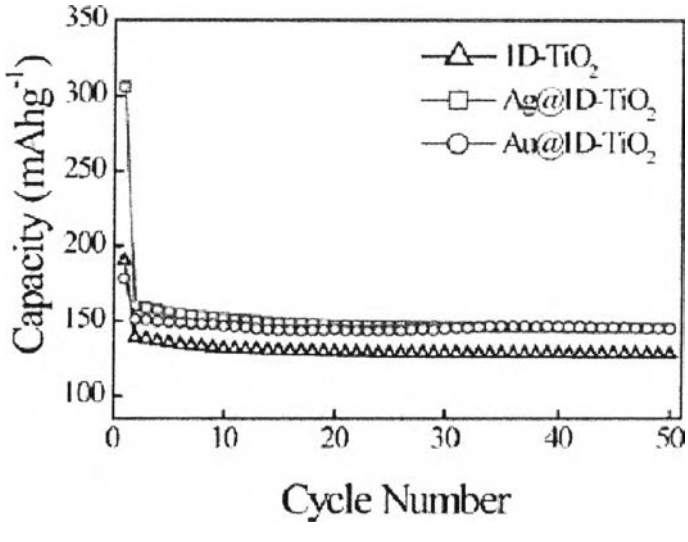

Figure 2.22 Cycle performance on the discharge capacities of the test cells at the constant current rate.

In 2010, Kanjwal *et al.* fabricated nanofibrous titanium oxide attached with zinc oxide nanobranches as an anode material, resulting in an improved performance of LIBs. ZnO-doped TiO_2 nanofibers were prepared by 3 steps. First, electrospinning of a zinc powder/Ti(Iso)/PVAc colloid was carried out to produce polymeric nanofibers embedding solid nanoparticles, followed by calcination of the electrospun nanofiber mats to eliminate the residue polymer and produce titanium oxide nanofibers doped with zinc oxide nanoparticles. The outgrowth of ZnO nanoparticles to be ZnO nanobranches on the surface of the titanium oxide nanofibers was then achieved by using a hydrothermal technique. The obtained nanostructure exhibited a high rate capacity of 1232 $mAhg^{-1}$ (see in Figure 2.24) that is suitable for high energy density LIBs with higher performance.

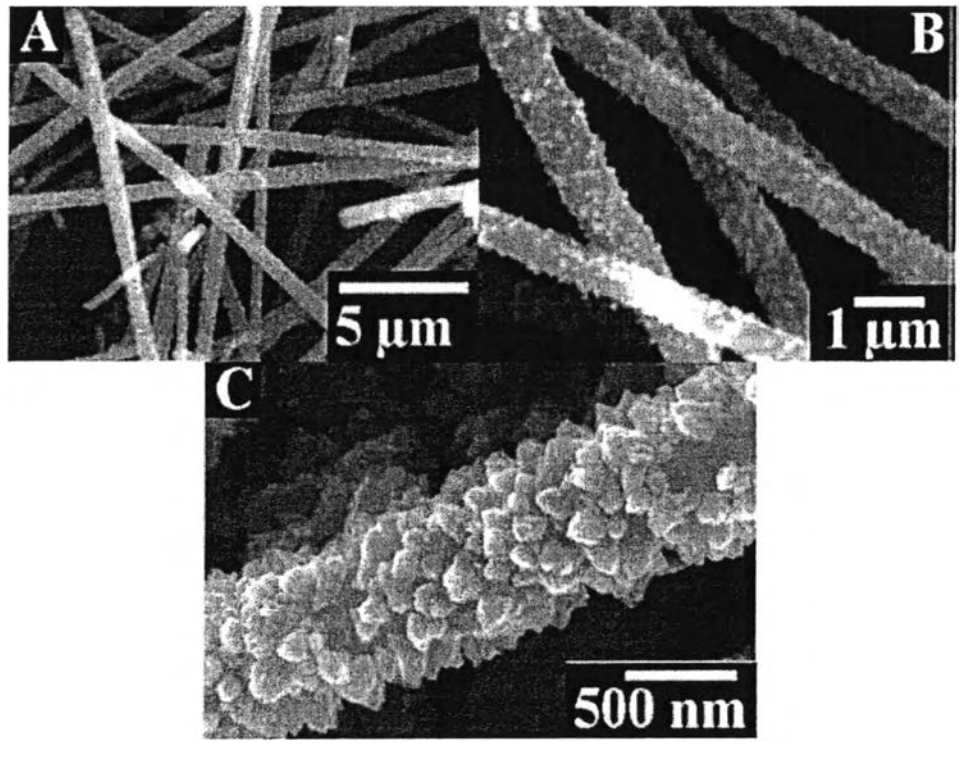

Figure 2.23 The SEM; (A and B) and FE-SEM; (C) images of hydrothermally treated nanofibers.

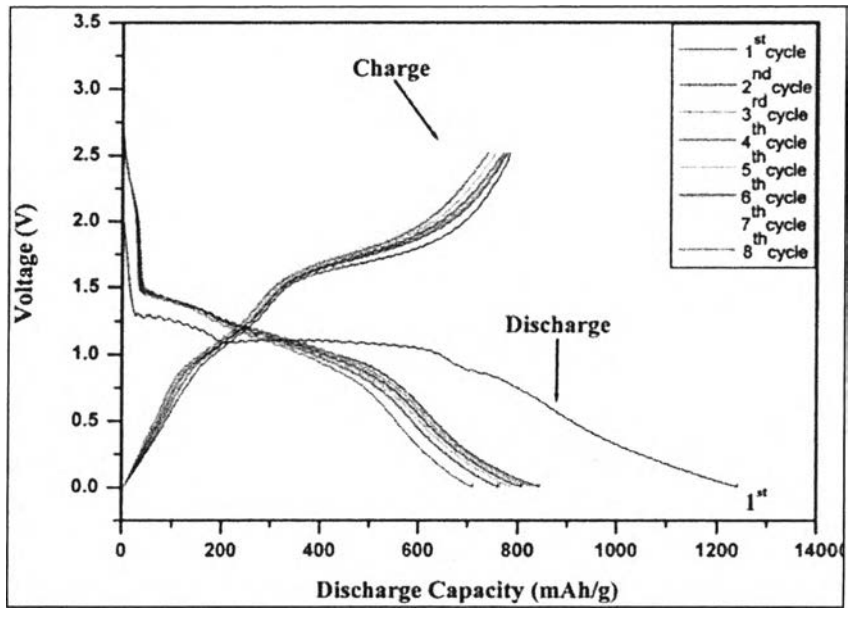

Figure 2.24 The galvanostatic charge-discharge curves for the prepared TiO_2-ZnO nanostructure.

Yang *et al.* (2011) explored the nanosized anatase titanium dioxide loaded porous carbon nanofibers (TiO_2/PCNFs) which was prepared from electrospun $TiO(OAc)_2$/PAN/PMMA composite precursor containing different amount of PMMA porogen, and subsequent thermal treatment. To compare with the TiO_2/CNFs, the TiO_2/PCNFs showed an outstanding higher improvement of cyclic reversible capacity due to the increased electrode surface area corresponding to their porous structure. Moreover, they found that the TiO_2/PCNFs fabricated from 3:1 mass ratio of PAN to PMMA exhibited the best high-rate performance with a high stable capacity retention of approx. 200 $mAhg^{-1}$ at a current density as high as 800 mAg^{-1}. This superior electrochemical performance of the TiO_2/PCNFs (PAN: PMMA=3:1) comes from the combined merits of the unique hollow-core structure of the PCNFs support and the homogeneous dispersion of the nanosized TiO_2.

ต้นฉบับ หน้าขาดหาย

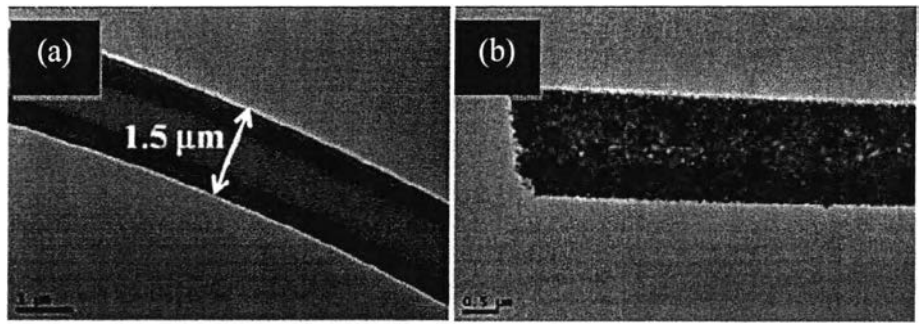

Figure 2.26 The TEM images (a) and (b) of the as-prepared nonwoven TiO_2 and TiO_2 /Ag films after calcination at 500 °C for 1 h in air respectively.

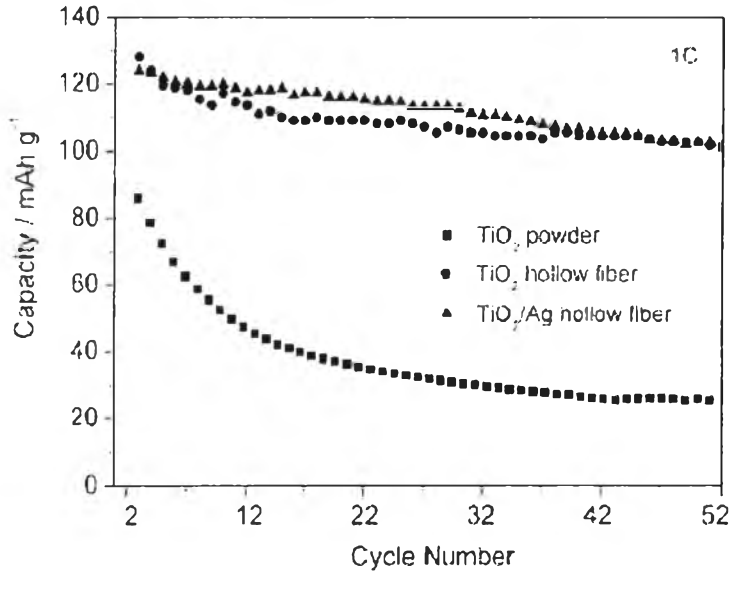

Figure 2.27 The Cycling behaviors of the anatase TiO_2 powder, TiO_2 and TiO_2 /Ag hollow fibers.

In 2012, Zhu *et al.* studied long term cycling of electrospun TiO_2 nanostructure and their composites with MWCNTs for rechargeable LIBs using electrospinning and subsequent sintering process. The obtained materials was found to show long term cycling stability and a stable performance up to 800 cycles, with capacity retention of 92% (10 to 800 cycles) and 81% (10 to 800 cycles) for TiO_2 nanofibers and TiO_2 rice grain nanostructures, respectively. Even though, capacity value of TiO_2–CNT (4 wt.%) composites insignificantly lower than those

two, they exhibited enhancement in the capacity retention (8% capacity loss between 10-800 cycles).

Also in 2012, The Si core/C shell nanofibers are synthesized by Lee *et al.* (2012) via co-axial electrospinning of Si nanoparticles in styrene-co-acrylonitrile core solution and poly(acrylonitrile) shell solution and subsequent thermal treatment. In situ observation of the contact-lithiation of the Si core/C shell nanofibers shows their mechanical durability during the electrochemical reactions, empowering the stable electrochemical performance of these nanofibers. The electrochemical performances of the composite anode are significantly improved by incorporating Si nanoparticles of 9.9 wt.% into the core of hollow carbon nanofibers. The capacity retention is 92% after 50 cycles.

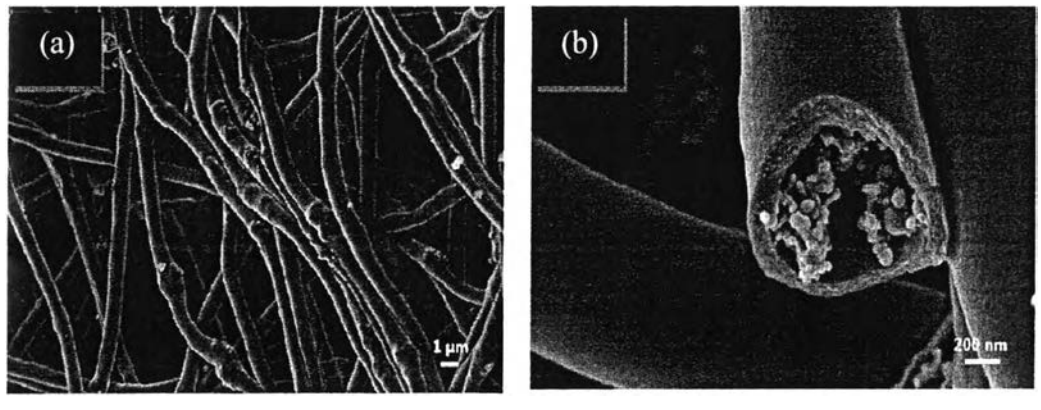

Figure 2.28 The FE-SEM images of Si core/C shell nanofibers: (a) low and and (b) high magnifications.